Nanodomain formation in a liquid polymer blend: The initial stages of phase separation

Andrew H. Marcus,[a] Deborah M. Hussey, Nathan A. Diachun, and M. D. Fayer
Department of Chemistry, Stanford University, Stanford, California 94305

(Received 3 June 1994; accepted 8 August 1995)

The morphology of nanodomain structures in binary polymer blends of a random copolymer and a homopolymer is determined using electronic excitation transport (EET) studies. The experimental system employed is a copolymer, 6.5% atactic poly(methyl methacrylate-*co*-2-vinyl naphthalene) [P(MMA-2VN)], in atactic poly(vinyl acetate) (PVAc). The naphthalene groups serve as chromophores in the EET experiments. The mixtures are prepared such that initially the P(MMA-2VN) chains are randomly distributed in the PVAc matrix. The nanodomains are formed while low-concentration mixtures of the P(MMA-2VN) in PVAc are held at constant temperature in the melt state ($T>T_g$), above the temperature at which phase separation occurs. In the melt the chains diffuse, and P(MMA-2VN) chains aggregate until the temperature is quenched below T_g. The structures of the resulting domains are examined with time-resolved fluorescence depolarization measurements, and the data are analyzed using an analytical theory to model EET among interacting polymer chains. The agreement between theory and data is very good. The results of the analysis indicate that the nanodomains correspond to aggregates with a characteristic size equal to the radius of gyration of the copolymer, R_g. The number of P(MMA-2VN) chains in aggregates prepared under different conditions is determined. © *1995 American Institute of Physics.*

I. INTRODUCTION

The details of molecular structure in polymeric solids is a topic of tremendous importance. Knowledge of structure at the molecular level is a necessary step toward a comprehensive statistical mechanical description of bulk polymer properties. Such an understanding can be employed to predict the physical properties of new materials, and to design materials with specific characteristics.

In the case of binary polymer blends, little is known about structure during the initial stages of phase separation. The phase separation studied in this work is a nonequilibrium transformation from an unstable homogeneous phase to a stable two-phase system. In the homogeneous phase, the blend's components are fully mixed on submolecular distance scales, while the phase-separated blend contains segregated domains of macroscopic dimension. Molecular segregation, however, can occur on distance scales much smaller than the minimum domain size associated with macroscopic phase separation. Macroscopic domains are large enough to observe directly by light microscopy or light scattering methods ($R_d \sim 1000$ to 10 000 Å), while nanodomains are too small to study by conventional techniques ($R_d \sim 10$ to 100 Å). A nanodomain is a region where as few as two or three polymer coils of one component have aggregated. The details of nanodomain structure and formation are not well understood. Nevertheless, it has been shown that nanodomains exist in solid blends which appear macroscopically homogeneous.[1–3]

Typically, the experimental methods employed to study phase separation are light scattering,[4,5] small angle neutron scattering (SANS),[6,7] NMR,[8,9] and structural characterization by microscopy[3,10,11] and digital image analysis.[12] Pioneering work on the kinetics and mechanisms of polymer phase separation has been carried out using microscopy[11] and pulsed NMR techniques.[9] Spinodal decomposition in binary polymer blends has been studied by Hashimoto and colleagues using time-resolved light scattering[4,5] and SANS[6] measurements. Spiess has used proton spin diffusion to examine the microphase structure of various polymer systems.[8] Of particular relevance to the work described below are the NMR and the SANS measurements, since they have been successfully used to probe submicron scale structure during the phase separation process. The most important limitation to the scattering techniques, however, is the necessity of introducing sufficient scattering contrast between the components or the phases comprising the blend. Usually this involves deuterating one of the components, which has the effect of altering the phase diagram. For example, in the case of deuterated poly(styrene) in poly(vinyl methyl ether), the critical temperature for phase separation is increased by 60 °C compared to that of the protonated blend.[10] Such thermodynamic differences between the deuterated and protonated systems have been studied for some time,[13,14] and do not detract from the fundamental information gained from such studies. SANS experiments become less useful in the limit of very low concentrations of scattering centers. This is the situation examined in this work. Probably the technique that is closest in spirit to this work is the NMR spin diffusion.[8] In the experiments described here, excitation diffusion is observed rather than spin diffusion. Examination of excitation diffusion provides enhanced sensitivity that is generally associated with optical experiments.

In recent years, electronic excitation transport (EET) studies of chromophores bound to polymers or to micelle assemblies have become a useful tool for the elucidation of macromolecular structure.[2,15–27] Since the emission of fluo-

[a]Current address: the James Franck Institute, The University of Chicago, Chicago, Illinois 60637.

rescence occurs against a dark background, it is possible to obtain high quality data from very low concentrations of light-emitting probe molecules (chromophores). Moreover, fluorescence measurements are a straightforward method for the examination of the excited-state dynamics associated with systems of interacting chromophores. Resonant dipolar coupling between the singlet electronic states of interacting chromophores was first described as a mechanism for EET by Förster.[28,29] The $1/r^6$ dependence of the transition dipole–transition dipole interaction has led to the determination of interchromophore distances that are directly related to the segmental distribution of macromolecules containing a small number of randomly distributed chromophores.[2,21,25] This is similar to the role nuclear dipolar relaxation (which also follows a $1/r^6$ dependence) has played in the determination of interatomic distances using nuclear Overhauser enhancement studies.[30] The distance sampled by the Förster interaction depends on the oscillator strengths of the chromophores and the spectral overlap between the excited singlet state of the donor and the ground state of the acceptor.[31] This interaction is characterized by the Förster transfer distance, R_0. Depending on the specific system, R_0 may range from 6 to 60 Å.[31]

Recently, analytical methods have been developed to describe EET among chromophores embedded in spatially complex systems.[18] The technique has been applied to experimental studies of concentrated micelle suspensions with chromophores restricted to the micelle surfaces,[17] and to pendant chromophores covalently bound to the backbones of interpenetrating polymer chains.[15] For the micelle system, the accuracy of the method has been confirmed by comparison to the results of Monte Carlo simulations.[16] In both experimental situations, EET occurs within a chromophore cluster, e.g., a micelle or a polymer coil, and between clusters.

The method makes use of a truncated cumulant approximation which is based on the assumption that the cumulative effect of all transfer processes is well described by a superposition of pairwise interactions.[32–36] In this way, the multiple step processes which occur in clustered systems may be partitioned into fast events internal to a cluster and the slower transfer steps between interacting clusters. This renormalizes a many-body problem into a tractable two-body problem that can be formulated analytically. Since the interaction between clusters is treated in analogy to the interaction between two ''effective chromophores,'' the technique is called the effective chromophore (EC) method.

The center-to-center coil-pair distribution is inherently nonrandom in a nanodomain structure formed in the initial stage of phase separation of a binary blend. In this work, we present experimental measurements of EET among the chromophore substituents of a copolymer [atactic 6.5% poly(methyl methacrylate-*co*-2-vinyl naphthalene), or P(MMA-2VN)] dispersed at low concentrations in a chemically distinct and optically inert polymer host [atactic poly(vinyl acetate), or PVAc]. Under the appropriate conditions, the chromophore-containing, minor component forms nanodomain structures that lead to an increase in the observed EET. The EC analysis is used to interpret the experimental observables in terms of highly correlated coil centers. Here, the center-to-center pair distribution, $g_{\mathrm{c.m.}}(r)$, has the physical meaning of the relative probability of finding two different molecular centers of the P(MMA-2VN) separated by the distance r.

The behavior of interacting clusters of chromophores can be understood as a superposition of EET processes which include both the EET in a single cluster (internal) and the EET between cluster pairs (external). Thus, the survival probability of an excited chromophore (probability that the initially excited chromophore is still excited at a time t after the initial excitation at $t=0$) will depend on transfer among chromophores on the same chain and on interchain transfer which increases in frequency as the number of chains in the nanodomain increases. Therefore, by measuring the survival probability [$G^s(t)$, see below] it is possible to determine properties of nanodomain structure as a function of the sample preparation conditions.

This paper is organized in the following manner: In Sec. II, we briefly discuss the application of the two-particle cumulant approximation to calculation of the EET observables obtained from nanophase-separated P(MMA-2VN)/PVAc systems. A general treatment of this problem has been reported previously.[18] Section III describes the experimental instrumentation and the preparative techniques employed. Section IV is a discussion of the results.

II. THEORY AND CALCULATION OF OBSERVABLES

In this section, we present a model for energy transport among identical chromophores randomly attached to the backbones of polymer coils in an amorphous binary blend. The formulation is similar to one presented in Ref. 15; however, here the effects of molecular aggregation are accounted for in the observables. We adopt a formalism which makes use of a truncated cumulant approximation to the Green's function solution of the Pauli master equation.[32,33] The time-dependent motion of an excitation within an ensemble of interacting chromophores can be characterized by the function $G^s(t)$.[37,38] $G^s(t)$ is the self-part of the Green's function. It represents the probability that the initially excited chromophore is still excited at some later time. $G^s(t)$ includes transfer events in which the excitation leaves the initial site and later returns, but does not include the excited state lifetime.

The usefulness of $G^s(t)$ lies in its relationship to the observables obtained from fluorescence depolarization experiments. A polarized excitation of an ensemble of randomly oriented chromophores results in a photoselected ensemble of excited states. Chromophores have a probability of excitation that depends on the angle between the E field of the light and the direction of their molecular transition dipole moment. Transfer of the excitation to surrounding molecules, which are randomly oriented, and subsequent emission leads to depolarization of the observed fluorescence. This results in fluorescence anisotropies dominated by $G^s(t)$, provided other depolarization processes (such as chromophore rotation) occur on a slower time scale. For the experiments presented here, we obtain high-resolution excited-state decay profiles polarized both parallel and perpendicular to the ex-

citation polarization. These decays are converted to fluorescence anisotropies, which are related to $G^s(t)$ for the polymer system.

The cumulant is truncated at first order. Therefore, all transfer events between chromophores are modeled by pairwise interactions. Approximations of this type display excellent agreement with more accurate representations of the Green's function for infinite isotropic systems as well as for restricted finite-volume systems.[21,25,32–35] The first-order cumulant approximation provides a mathematically tractable approach to the complex problem examined here.

We describe the excitation dynamics in polymer systems by separating $G^s(t)$ into two contributions, $G^s_{\rm on}(t)$ and $G^s_{\rm off}(t)$.[18] $G^s_{\rm on}(t)$ describes transport ''on'' the coil containing the originally excited chromophore. This part of the energy transport is internal to the coil, corresponding to the zeroth-order term of a cumulant in coil density. $G^s_{\rm off}(t)$ describes forward- and back-transfer from the originally excited coil to chromophores on neighboring coils. This part of $G^s(t)$ represents an interaction between coil pairs and corresponds to the first-order term of the cumulant. In the context of this model, all transfer events are independent. That is, the probability of transfer to other coils is unaffected by the probability of transfer within a coil. This implies that the ensemble average decay of the Green's function can be written $\langle G^s(t)\rangle = \langle G^s_{\rm on}(t)\rangle\langle G^s_{\rm off}(t)\rangle$.[18,39] Thus, the observed excitation transfer in a concentrated sample of chromophore-containing coils can be viewed as the low concentration dynamics (isolated coils) modified by the dynamics due to intercoil EET. We are then faced with the separate problems of calculating $\langle G^s_{\rm on}(t)\rangle$ and $\langle G^s_{\rm off}(t)\rangle$.

A. Microsystem calculations: Chromophores distributed within two Gaussian surfaces

Consider two identical polymer coils with radius of gyration R_g, separated by the distance R_s. Both coils have chromophores randomly oriented and distributed along their backbones. One is designated the ''donor coil'' while the other is the ''acceptor coil.'' The intercoil separation may be large so that the segments of the two molecules do not come into contact, or small so that the segments interpenetrate extensively. We examine the case in which a single chromophore on the donor coil is excited and incoherent energy transfer to surrounding unexcited chromophores can occur by a dipole–dipole type mechanism.[28]

In general, the ensemble average decay of the excitation probability of a donor molecule surrounded by a distribution of acceptors is given by,[18,35]

$$\ln\langle G^s(t)\rangle = -\frac{\rho}{2}\int_{\rm space}\{1-\exp[(-2t/\tau)\times(R_0/|\mathbf{r}|)^6]\}u_a(\mathbf{r})d\mathbf{r}. \tag{2.1}$$

Here, ''donor'' means the initially excited molecule, while ''acceptors'' refers to unexcited but otherwise identical molecules. In Eq. (2.1) ρ represents the number density of acceptor molecules, τ is the excited state lifetime, R_0 is the characteristic Förster transfer distance, and $\mathbf{r}$ is the vector which spans the volume of the chromophore distribution. The vector distribution $u_a(\mathbf{r})$ is defined such that $\rho u_a(\mathbf{r})d\mathbf{r}$ is the fraction of acceptors in the region between $\mathbf{r}$ and $\mathbf{r}+d\mathbf{r}$. The normalization condition is

$$\rho\int_{\rm space} u_a(\mathbf{r})d\mathbf{r} = (N-1), \tag{2.2}$$

where N is the total number of chromophores (donor and acceptors) within the finite volume. The integrals in Eqs. (2.1) and (2.2) are carried over the space containing the donor and acceptor chromophores.

Equation (2.1) describes the excitation decay of a single donor molecule on the donor coil interacting with a distribution of chromophores on the acceptor coil. Since the distribution of acceptor chromophores depends on the original donor position, Eq. (2.1) must be averaged over the space of the donor coil:

$$\langle G^s(t)\rangle = \frac{1}{V_d}\int_{\rm space}\langle G^s(t,\mathbf{r}_d)\rangle u_d(\mathbf{r}_d)d\mathbf{r}_d, \tag{2.3a}$$

$$\langle G^s(t,\mathbf{r}_d)\rangle = \exp\left(-\frac{(N-1)}{2V_a}\int_{\rm space}\{1-\exp[(-2t/\tau)\times(R_0/|\mathbf{r}_{ad}|)^6]\}u_a(\mathbf{r}_a)d\mathbf{r}_a\right). \tag{2.3b}$$

In Eqs. (2.3) the volumes V_d and V_a are those occupied by the donor and acceptor distributions. The vector $\mathbf{r}_{ad}$ joins the positions of the acceptor and donor chromophores.

To perform the integrals in Eqs. (2.3), we adopt a multiframe coordinate system. The space containing the donor and acceptor distributions is spanned by the vectors $\mathbf{r}_1$ and $\mathbf{r}_2$, respectively. The donor–acceptor separations are then given by a coordinate transformation[13] that depends on the distance between the coil centers of mass. Thus, $\mathbf{r}_2 = Ar'_{12}$, where r'_{12} spans the space containing the acceptor molecules in a newly defined coordinate system. The donor and acceptor distributions are modeled as Gaussian functions after the Gaussian chain model:[10]

$$u_d(\mathbf{r}_1) = \left(\frac{3}{2\pi\langle R_g^2\rangle}\right)^{3/2}\exp\left(\frac{-3}{2\langle R_g^2\rangle}r_1^2\right), \tag{2.4a}$$

$$d\mathbf{r}_1 = r_1^2\sin\theta_1\,dr_1\,d\theta_1\,d\phi_1, \tag{2.4b}$$

$$u_a(\mathbf{r}_2) = \left(\frac{3}{2\pi\langle R_g^2\rangle}\right)^{3/2}\exp\left(\frac{-3}{2\langle R_g^2\rangle}r_2^2\right), \tag{2.4c}$$

$$d\mathbf{r}_2 = r_2^2\sin\theta_2\,dr_2\,d\theta_2\,d\phi_2. \tag{2.4d}$$

Substitution of Eqs. (2.4) into Eqs. (2.3) and further simplification by symmetry arguments result in

$$\langle G^s_{\rm off}(t,R_s)\rangle = 2\pi\left(\frac{3}{2\pi\langle R_g^2\rangle}\right)^{3/2}\int_{r_1}\int_{\theta_1} G^s(r_1,\theta_1)\times\exp\left(\frac{-3}{2\langle R_g^2\rangle}r_1^2\right)r_1^2\sin\theta_1\,dr_1\,d\theta_1, \tag{2.5a}$$

$$\ln[G^s(r_1,\theta_1)]$$
$$=(N-1)\pi\left(\frac{3}{2\pi\langle R_g^2\rangle}\right)^{3/2}\int_{r_2}\int_{\theta_2}\Bigg\{\exp[(-2t/\tau)$$
$$\times(R_0/(r'_{12}(\theta_1,\theta_2,r_1,r_2))^6]-1\Bigg\}\exp\left(\frac{-3}{2\langle R_g^2\rangle}r_2^2\right)r_2^2$$
$$\times\sin\theta_2\,dr_2\,d\theta_2, \tag{2.5b}$$

where

$$|r'_{12}(\theta_1,\theta_2,r_1,r_2)|^2=r_1^2+r_2^2+2R_s[r_2\cos\theta_2 - r_1\cos\theta_1]-2r_1r_2\cos(\theta_2-\theta_1)+R_s^2. \tag{2.5c}$$

Equations (2.5) express the excitation dynamics between two coils separated by the distance R_s. In the limit of vanishingly small R_s, the donor and acceptor distributions superimpose, and the resulting excitation dynamics occur as if on a single, isolated coil. That is, $\langle G^s_{\rm off}(t,0)\rangle = \langle G^s_{\rm on}(t)\rangle$. For all finite separations, these integrals must be evaluated numerically.

Thus far, we have derived $\langle G^s(t)\rangle$ for two specific cases: $\langle G^s_{\rm on}(t)\rangle$ describes excitation transfer among N chromophores on a single isolated coil, while $\langle G^s_{\rm off}(t)\rangle$ [Eqs. (2.5)] describes excitation transfer between a donor chromophore on a ''donor coil'' and N-1 acceptor chromophores on an ''acceptor coil,'' where the two coils are separated by the distance R_s. $\langle G^s_{\rm off}(t)\rangle$ contains the details of the chromophore distributions, and it represents the configurational average of the transport dynamics due to the pairwise interaction between two coils. These two descriptions of the coil transport dynamics, which separately contain internal and coil–pair interactions, are sufficient to model the copolymer concentration-dependence of $G^s(t)$.

B. Calculations for chromophore-containing copolymer aggregates

An extension of Eqs. (2.5) to experimental observables must consider the effect of molecular interactions on both the intramolecular structure and the intermolecular radial distribution function. A complete description of the bulk structure would include the complex interdependencies of the possible intra- and intermolecular conformations. In the case of a bulk homopolymer, it is possible to make use of the fact that individual coils in single-component dense melts and glasses are ideal.[40,41] The concept of a Θ condition in condensed, disordered, single-component homopolymers has been repeatedly verified in the literature.[42,43] In these situations, the forces which lead to intramolecular excluded volume are balanced by those forces arising from the interactions between molecules. The Flory postulate states that the segmental distribution of an ideal chain (Θ condition) is Gaussian for distances beyond a few statistical segment lengths with a second moment that scales linearly with the chain size.[44] Since the copolymer chains in these experiments contain only a small number of chromophores (less than one chromophore per statistical segment length), the average interchromophore separation is large enough for the energy-transport observable to reflect global chain structure in the experimental system studied.[1] Furthermore, a previous study in which a Gaussian model was assumed has shown that low naphthyl concentrations in the copolymer do not cause the R_g to differ in a detectable manner from that of PMMA.[1] Therefore, it is reasonable to assume an ideal Gaussian distribution for the individual copolymer coil configurations in bulk PMMA. In Ref. 15, the Gaussian chain model was successfully employed to obtain an analytic description of the excitation dynamics of the copolymer in PMMA.

For a binary blend of P(MMA-2VN) in PVAc, however, the situation is far removed from one described by a Θ condition. The component species in binary blends may differ in various local and global structural features as well as interact through attractive or repulsive dispersivelike forces.[44,45] Nevertheless, it is possible to model such binary systems by considering mixtures of Gaussian chains.[45] Such studies have successfully explained SANS measurements of polymer mixtures that exhibit phase-separation behavior.[7,13]

We proceed by averaging Eqs. (2.5) over intermolecular radial separations relevant to the energy transport observable. Since the coils are believed to form nanodomains, the coil centers of mass are constrained to lie in the space of a finite volume. Thus, the cluster-to-cluster ''effective chromophore'' interaction described by Eqs. (2.5) can be treated in exact analogy to the Förster interchromophore interaction for chromophores distributed in a finite volume. Equations (2.3) are rewritten

$$\langle G^s_{\rm off}(t,N_c)\rangle=\frac{1}{V}\int_{\rm space}\langle G^s_{\rm off}(t,N_c,\mathbf{R}_d)\rangle u(\mathbf{R}_d)d\mathbf{R}_d, \tag{2.6a}$$

$$\langle G^s_{\rm off}(t,N_c,\mathbf{R}_d)\rangle=\exp\left(-\frac{(N_c-1)}{2V}\int_{\rm space}[1-\langle G^s_{\rm off}(t,R_s)\rangle]u(\mathbf{R}_a)d\mathbf{R}_a\right), \tag{2.6b}$$

where $\mathbf{R}_d$ and $\mathbf{R}_a$ are the center-of-mass positions of the donor and acceptor coils, respectively, $R_s=|\mathbf{R}_d-\mathbf{R}_a|$, the spatial distributions of the donor and acceptor coils are indistinguishable, and N_c is the total number of chromophore-containing coils in the nanodomain cluster. In Eqs. (2.6), $u(\mathbf{R})d\mathbf{R}$ represents the probability that the center of mass of a copolymer molecule (modeled as a symmetric, Gaussian function) lies between the radial distances $\mathbf{R}$ and $\mathbf{R}+d\mathbf{R}$ from the nanodomain's center of mass. The form of $u(\mathbf{R})$ serves to characterize the intermolecular nanodomain structure. As discussed in Sec. IV, the average nanodomain concentration (mean aggregation number) is the only adjustable parameter in the data analysis. Therefore, certain considerations that influence the selection of $u(\mathbf{R})$ will be discussed in Sec. IV as well.

A distribution function, $P(N_c)$, is used to describe the probability of finding N_c chromophore-containing copolymer coils in a given domain. In general, the distribution will depend on the effect of dispersive forces between the coils. For the simplest case, $P(N_c)$ is given by the Poisson distribution. The Poisson average of Eq. (2.6a) is

TABLE I. Physical characteristics of the guest [6.5% atactic poly(methyl methacrylate-*co*-2-vinyl naphthalene)] copolymer in PMMA and PVAc hosts. M_w is the weight-average molecular weight, M_w/M_n is the polydispersity, %2-VN is the number percent of naphthyl subunits, $\langle N_{\text{chrom}}/\text{coil}\rangle$ is the average number of chromophores per molecule, N_{mon} is the number of monomers per molecule, N_{stat} is the number of statistical segments per molecule, l_{stat} is the statistical segment length, and $\langle R_g^2\rangle^{1/2}$ is the rms radius of gyration based on the random chain model. Measurements of the values shown for $\langle R_g^2\rangle^{1/2}$ is the subject of Ref. 21.

Host	M_w	M_w/M_n	%2-VN	$\langle N_{\text{chrom}}/\text{coil}\rangle$	N_{mon}	N_{stat}	l_{stat}	$\langle R_g^2\rangle^{1/2}$
PMMA	25,300	1.55	6.5	16	244	39	15.9 Å	40.5 Å
PVAc	25,300	1.55	6.5	16	244	39	13.3 Å	34 Å

$$\langle G^s_{\text{off}}(t,\nu)\rangle = \sum_{N_c=0}^{\infty} \frac{N_c}{\nu}\left(\frac{e^{-\nu}\nu N_c}{N_c!}\right)\langle G^s_{\text{off}}(t,N_c)\rangle, \qquad (2.6c)$$

where ν is the mean number of chromophore-containing coils per domain.

Equations (2.6) describe the decay of excitation probability in a solution of chromophore-containing copolymer clusters (with a Poisson average of ν copolymer coils per cluster) due solely to intercoil transfer events. The intracoil transfer, which is present for all values of ν, contributes to the overall decay according to $\langle G^s(t,\nu)\rangle = \langle G^s_{\text{on}}(t)\rangle \times \langle G^s_{\text{off}}(t,\nu)\rangle$.[18] According to Eq. (2.6), $\langle G^s_{\text{off}}(t,\nu)\rangle$ approaches a time-independent value of unity as the coil concentration approaches zero. This allows the overall decay of $\langle G^s(t,\nu)\rangle$ to approach $\langle G^s_{\text{on}}(t)\rangle$ with decreasing aggregation, as expected.

The function G^s represents the probability of irreversible decay of an excitation due to energy transfer. Its relationship to the fluorescence anisotropy, which contains all sources of depolarization, can be written as

$$r(t,\nu) = \langle \Phi(t)\langle G^s(t,\nu)\rangle\rangle. \qquad (2.7)$$

Here, $\Phi(t)$ contains processes besides energy transport which contribute to the depolarization. The most important of these is molecular reorientation, which occurs on a much slower time scale than that of the energy transport we wish to observe. The outer brackets in Eq. (2.7) indicate a configurational average that includes correlations between $\Phi(t)$ and the energy transport. The difference in their time scales, however, suggests that the correlations are insignificant, and that the excitation transfer is independent of molecular rotation. Thus, Eq. (2.7) can be rewritten as

$$r(t,\nu) = \exp(-t/\tau_{\text{rot}})\langle G^s(t,\nu)\rangle \qquad (2.8)$$

where τ_{rot} is the rotational correlation time.

III. EXPERIMENTAL METHODS

A. Sample preparation

A copolymer comprised of 93.5% methyl methacrylate (MMA) and 6.5% 2-vinyl naphthalene (2-VN) was prepared using the methods described by Peterson *et al.*[1] The fraction of 2-VN subunits in the copolymer was determined by measuring the absorbance of a known quantity of the material dissolved in CH_2Cl_2. The concentration of substituted naphthalene was determined based on the molar extinction coefficient for 2-ethyl naphthalene (350 $M^{-1}\,cm^{-1}$ at 320 nm). This polydisperse material (M_w=36 900, M_w/M_n=2.16) was fractionated by size-exclusion chromatography using a preparative gel permeation chromatograph (GPC) fitted with a Polymer Laboratories PL gel resin 500 Å column. Toluene was the eluent. The molecular weights and polydispersities of the fractions were determined with a Waters Associates' analytical GPC, using THF as eluent.

The physical characteristics of the guest copolymer used in this study are reported in Table I. This particular fraction was chosen to emulate a previous study of EET in isolated P(MMA-2VN) coils in a PVAc host.[21] The host PVAc(M_w=83 000, M_w/M_n=2.1) was purchased from Aldrich Chemical and used as received. All weights were measured using a Gram–Attic balance (Fischer Scientific Company) accurate to within ±0.0001 g. Volumes were measured with calibrated volumetric flasks and pipettes.

The samples were made as consecutive dilutions of a concentrated sample. A stock solution of 15% host PVAc in benzene was prepared. An aliquot of this solution was combined with a measured quantity of the guest copolymer to make a 10% guest/host mixture. Less concentrated samples (5%, 2.5%, 0.31%, 0.15%, and 0.05%) were made by consecutive dilution of the 10% solution. These polymer/benzene solutions were then freeze-dried by immersion in liquid nitrogen, followed by sublimation of the frozen benzene under vacuum.

Optical quality samples were obtained by compression-molding the freeze-dried material above the glass transition temperature of the blend. The procedure was similar to that used by Ediger[2] and Peterson,[1] although there were some notable differences. The freeze-dried material was loaded into a Specac heatable die cell with polished stainless steel platens. This die cell was sealed in an aluminum bag which was subsequently purged with nitrogen gas. The bag and die cell were placed between the heated platens of a Carver die press. The temperature of the sample was monitored using a thermocouple inserted into the base of the die. After the sample temperature was held between 82 °C–87 °C for a particular annealing time, the die was pressed to 0.5 metric tons for 2 min. The die cell was immediately removed from the hot Carver press and quenched in dry ice. All samples were made with an appropriate width (see Tables II and III) to insure an optical density below 0.2 at the peak absorption wavelength (320 nm). The optical quality of the samples was checked using a polarizing microscope. The samples were found to be optically clear (incapable of scattering visible light) and free of birefringence.

Two series of solid solutions were prepared and are presented in Tables II and III, respectively. In series *A*, the annealing time was held constant (t=20 min), while the initial

TABLE II. Series A: Concentration-dependent samples. Vol. % is the copolymer volume percent, t_{an} is the annealing time, τ_F is the measured fluorescence lifetime, width is the sample thickness, and O.D. is the measured optical density at the absorption maximum (λ_{max}=320 nm).

Vol. %	t_{an} (min)	τ_F (ns)	Width (mm)	O.D.
10.0	20	43.4	0.11	0.12
5.0	20	46.1	0.15	0.16
2.5	20	45.1	0.26	0.14
0.31	20	49.8	2.5	0.16
0.15	20	51.5	5.0	0.16
0.05	20	51.2	6.0	0.05

concentration of the copolymer was varied ($0.05\% \leqslant c_0 \leqslant 10\%$). In series *B*, all samples contained an identically low concentration of the chromophore-containing copolymer (c_0=0.31%), but the annealing time was varied ($0 < t \leqslant 16$ h). In both series, the samples were annealed at similar temperatures ($T=85\pm3$ °C).

In addition to the copolymer described above, a high-M_w PMMA (50 000 D, M_w/M_n=1.31) and a low-M_w PMMA (16 500 D, M_w/M_n=1.47) were each used as purchased from Scientific Polymer Products, Inc. in binary blends with the host PVAc for cloud-point measurements. Blends were prepared in several weight ratios by dissolution of PVAc and PMMA or P(MMA-2VN) in benzene at 5% total polymer weight/benzene volume, thorough mixing and lyophilization. Dry blend was loaded into the die cell of a Carver press at room temperature, evacuated, pressed to 0.5 metric tons, and transferred into a cloud-point cell. This method of sample preparation was chosen to match that for the time-resolved fluorescence anisotropy measurements as closely as possible.

B. Cloud-point measurements

Cloud-point measurements were conducted in calibrated, insulated, temperature-controlled copper cells with sapphire windows. Care was taken to be sure that the measured temperature was actually the temperature of the sample. The temperature was raised at a variety of rates to determine an appropriate heating ramp. The first hint of opalescence was detected with the aid of a microscope and backscattered illumination, and the temperature at which it occurred was identified as the cloud point. Samples of masses from 20.0 to 191.0 mg and thicknesses from 0.5 to 1.80 mm were studied to check for the dependence of the observed cloud points on sample thickness; no such dependence was found. Because the samples in which we observed nanoscopic aggregation (discussed below) were low concentration P(MMA-2VN)/PVAc blends, we focused on mapping the low copolymer content portion of the cloud-point curve, and for comparison, the low PMMA content portion of the cloud-point curve.

TABLE III. Series B: Annealing time dependent samples. Vol. % is the copolymer volume percent, t_{an} is the annealing time, τ_F is the measured fluorescence lifetime, width is the sample thickness, and O.D. is the measured optical density at the absorption maximum (λ_{max}=320 nm).

Vol. %	t_{an} (min)	τ_F (ns)	Width (mm)	O.D.
0.31	20	44.0	0.65	0.092
0.31	60	41.3	0.63	0.092
0.31	240	42.2	0.63	0.092
0.31	960	40.7	0.63	0.092

TABLE IV. Cloud-point temperatures for blends of PMMA and P(MMA-2VN) in PVAc (M_w=83 000).

Vol. %	PMMA (M_w=50 000)	PMMA (M_w=16 500)	P(MMA-2VN) (M_w=25 300)
10.0	89 °C	77 °C	~
5.0	91 °C	79 °C	⩽65 °C
2.5	93 °C	81 °C	⩽65 °C

Samples of PMMA/PVAc were studied with PMMA concentrations of 10%, 5%, and 2.5%. After trying increasingly slow heating ramps, it was determined that reliable results could be obtained using a heating ramp of 2 °C every 2 h, starting at 65 °C. These results are presented in Table IV. Cloud-point curves for PMMA/PVAc blends generated by Qipeng[46] with heating ramps from 2 to 20 °C per minute lie well above (roughly 100 °C) the cloud points observed in this work. In Ref. 46, it was pointed out that homogeneous samples held at temperatures 15 °C below the reported cloud-point curves became turbid after only 10 min. This illustrates the fact that the observed cloud point depends significantly on the heating ramp. We believe that the results reported here are reasonable approximations to the true equilibrium critical solution temperatures. However, because the observed cloud points are not far above the glass-transition temperatures, kinetic effects may still be slightly influencing the results.

The copolymer, while essentially identical to PMMA in its isolated coil structure, displays different phase-separation behavior in PVAc blends. The cloud-point results for the copolymer/PVAc blends are shown in Table IV for 5% and 2.5% samples. The cloud point was observed to occur after holding the samples at 65 °C for 3 h. This temperature is slightly above the glass-transition temperatures (~55 °C) of the blends. Macroscopic viscous flow was also observed to occur at 65 °C. Because of the very close proximity to the glass transition, it is not certain that this is the equilibrium critical solution temperature. The equilibrium critical solution temperature is clearly ⩽65 °C. Regardless of the exact value of the equilibrium critical solution temperature, it is clear that the samples used in the EET studies discussed below, annealed at 85 °C, were prepared above the equilibrium critical solution temperature, i.e., they were prepared in the phase-separated region of the phase diagram.

C. Time-resolved fluorescence measurements

Absorption spectra of the samples were measured using an Hewlett Packard 8452A diode array spectrophotometer. Time-resolved fluorescence anisotropy decays were measured using time correlated single photon counting. The apparatus and technique are described in detail elsewhere.[21,47] The excitation pulses were provided by the cavity-dumped output of a synchronously pumped dye laser tuned to 640 nm and frequency doubled to 320 nm. The pulse repetition rate

was 823 kHz, the pulse duration was ~10 ps and typical pulse energies after doubling were ~1 nJ. The excitation intensity was attenuated so that one fluorescent photon was detected for every 80 incident excitation pulses. Fluorescent photons were detected from the front face of the samples using an Hamamatsu microchannel plate in combination with a subtractive double monochromator tuned to 337 nm. The instrument response function (~50 ps FWHM) for this apparatus was recorded periodically during data collection, and the data were analyzed using the corresponding instrument response function.

Time-dependent decays of the polarized components of fluorescence, $I_{\parallel}(t)$ and $I_{\perp}(t)$, were collected in the following manner. A detection polarizer was held fixed while a Pockels cell was used to switch the plane polarization of the excitation beam between horizontal and vertical orientations. Each orientation was sampled for equal amounts of time, changing the polarization direction every 20 s. This procedure minimized the effect of laser instabilities over long periods of time as well as any inherent bias in the detection system.

Data-sets were collected for a duration such that the peak of each decay contained approximately 45 000 counts. The fluorescence anisotropy was then calculated by point-by-point addition and subtraction of the fluorescence decays,

$$r(t)=\frac{I_{\parallel}(t)-I_{\perp}(t)}{I_{\parallel}(t)+2I_{\perp}(t)}. \tag{3.1}$$

D. Data analyses

Theoretical anisotropies were calculated using Eqs. (2.5), (2.6), and (2.8) and compared directly with the data. The choice of time zero was made by matching the rising edge of both the data and the measured instrument response functions. The time corresponding to the peak of the instrument response (typically, 3/4 up the rising edge of a data set) was taken as time zero.

IV. RESULTS AND DISCUSSION

It is evident from Eqs. (2.5) that the necessary parameters for the cumulant approximation are the Förster critical transfer distance and the rms radius of gyration of the chromophore-containing copolymer. The dynamic Förster distance for 2-ethyl naphthalene dispersed in PMMA and in PVAc was previously determined to be 13.0 ± 0.6 Å for both host materials.[2,21] The orientation-dependent transfer distance is then obtained by multiplying the dynamic R_0 by the factor $(\gamma)^{1/3}(=0.9461)$, which is determined by performing the proper average over angles.[1,35] The rms radius of gyration is determined from the molecular weight provided both the statistical segment length (l_{stat}) and the number of statistical segments (N_{stat}) are known:

$$\langle R_g^2\rangle=\tfrac{1}{6}N_{\mathrm{stat}}(l_{\mathrm{stat}})^2. \tag{4.1}$$

The number of statistical segments is obtained from the relation, $N_{\mathrm{stat}}l_{\mathrm{stat}}=N_{\mathrm{mon}}l_{\mathrm{mon}}$, where N_{mon} and $l_{\mathrm{mon}}(\cong 2.54$ Å) are the number of monomers and the monomer length, respectively. The statistical segment length for several copolymers of 2-VN and MMA with various molecular weights has been determined by Peterson *et al.*[1,21] This value ($l_{\mathrm{stat}}=15.87$ Å) was established using EET measurements on isolated, chromophore-containing copolymers in bulk PMMA. It corresponds to radii of gyration identical to those obtained by light scattering measurements of polymer chains with identical molecular weights dissolved in Θ solvents. The corresponding statistical segment length of the copolymer dispersed in bulk PVAc ($l_{\mathrm{stat}}=13.3$ Å) was determined in a similar way by Peterson *et al.*[21] Figure 1 reproduces data and theoretical calculations from that work. The function $\langle G^s(t)\rangle$ was extracted from time-resolved fluorescence anisotropy measurements of the chromophore-containing copolymer ($M_w=25\,300$) dispersed in either of the host polymers. The decay of $\langle G^s(t)\rangle$ is faster in the PVAc host than in the PMMA. Analysis of these experiments established that the P(MMA-2VN) coils are collapsed relative to their radius of gyration observed under Θ conditions. It has also been determined that for the small fraction of 2VN in the copolymer used, l_{stat} is independent of that fraction, i.e., it is the same as that of the PMMA homopolymer.[21] Table I lists the rms radii of gyration for the copolymer used in the present study in both PMMA and PVAc hosts based on this information.

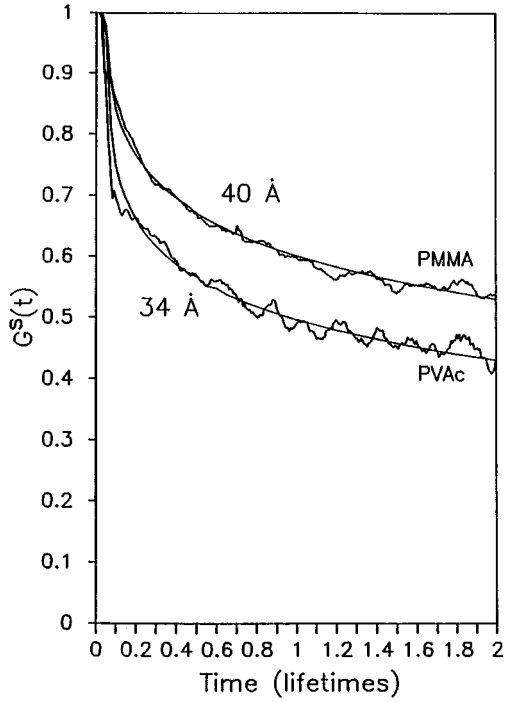

FIG. 1. Experimental measurements and a theoretical model of $\langle G^s(t)\rangle$ are shown for isolated molecules of P(MMA−2VN) in two different host materials: PMMA and PVAc.[21] The molecular weight of the P(MMA−2VN) is 26 000, similar to the molecular weight of the copolymer used in the present study. The decay of $\langle G^s(t)\rangle$ is faster for isolated molecules in PVAc than in PMMA, indicating that individual coils are partially collapsed in the blend ($R_g=34$ Å), while PMMA acts as a θ solvent ($R_g=40$ Å).

Having reliable values for both the Förster transfer distance and the radius of gyration, we can calculate the copolymer concentration dependence of the EET for any choice of the function, $u(\mathbf{R})$, describing the distribution of copolymer coils in a nanodomain. In order to choose a reasonable model

for $u(\mathbf{R})$, it is necessary to examine the experimental situation in more detail.

Before the samples used for EET studies are annealed, they are prepared in an unstable glassy state. The copolymer molecules are randomly dispersed (and kinetically trapped) in the host matrix with the initial concentration, c_0. When the temperature is raised above the blends T_g, the system becomes fluid and the molecules of both components diffuse throughout the material. In the fluid state, the system can approach equilibrium by forming aggregates when copolymer molecules encounter one another. Aggregation may continue during the annealing period until the material is quenched below the glass transition temperature. The samples are quenched prior to the establishment of equilibrium. The quenched material represents a snapshot of the aggregation process.

The work of Debye can provide us with a reasonable model for $u(\mathbf{R})$. According to Debye's thermodynamic theory of nonhomogeneous solutions of simple liquids,[48] the measurable effect of angular dissymmetry (critical opalescence) resulting from concentration fluctuations near the critical temperature is determined by an effective length, l. l is the range of molecular interaction between two molecules. In Debye's notation, it is defined by the relation

$$l^2=\frac{\int r^2\epsilon(r)d\mathbf{r}}{\int \epsilon(r)d\mathbf{r}}, \tag{4.2}$$

where $\epsilon(r)$ is the potential energy between two molecules separated by the distance r. In effect, two molecules separated by a distance larger than l do not influence one another energetically. For concentrated polymer solutions, Debye determined that l is equal to the radius of gyration of the polymer molecule, and that concentration fluctuations on this distance scale, which is much larger than that of ordinary molecules, will appear at temperatures removed from the critical point. This assertion was later validated experimentally,[49,50] and has subsequently been made use of by other workers.[49,51]

It is necessary to characterize $u(\mathbf{R})$ with two parameters: a size and a functional form. Following Debye, it is reasonable to assume that the size of the aggregates, at least during the initial stages of their growth, is determined by the parameter l. This is given by the radius of gyration of the copolymer. Since the isolated chains are essentially Gaussian in shape, as a reasonable approximation the domains are modeled as Gaussian distributions:

$$u(\mathbf{R})=\left(\frac{3}{2\pi\langle Rg^2\rangle}\right)^{3/2}\exp\left(\frac{-3R^2}{2\langle Rg^2\rangle}\right); \tag{4.3a}$$

$$d\mathbf{R}=R^2\sin\theta\, dR\, d\theta\, d\phi. \tag{4.3b}$$

$\langle G^s_{\rm off}(t,\nu)\rangle$ curves were constructed by numerically integrating the intercoil decays, $\langle G^s_{\rm off}(t,R_s)\rangle$, using Eqs. (2.6) and (4.3). These in turn were used to make theoretical anisotropies according to

$$r(t,\nu)=\Phi(t)\langle G^s_{\rm on}(t)\rangle\langle G^s_{\rm off}(t,\nu)\rangle. \tag{4.4}$$

Here, $\Phi(t)$ represents the fluorescence anisotropy decay due to rotation of the naphthyl chromophores, and $\langle G^s_{\rm on}(t)\rangle$ is that due to intracoil EET. Both $\Phi(t)$ and $\langle G^s_{\rm on}(t)\rangle$ were measured by Peterson *et al.*[21] The cumulant solution for $\langle G^s_{\rm on}(t)\rangle$ corresponding to $R_g=34$ Å (see Fig. 1) was used in Eq. (4.4). The isolated coil data is obtained from the most dilute sample ($c_0=0.05\%$). The functional form of $\Phi(t)$ (see Fig. 5 of Ref. 21) was obtained from a linear fit to the measured rotational anisotropy:

$$\Phi(t)=-0.007t+0.2, \quad \text{if } 0\leqslant t<4 \text{ ns};$$
$$\Phi(t)=-0.0002t+0.171, \quad \text{if } 4\leqslant t<100 \text{ ns}. \tag{4.5}$$

The fluorescence lifetimes of all the samples were determined from the total fluorescence, $I_{\rm tot}(t)=I_{\parallel}(t)+2I_{\perp}(t)$. These decays were single exponential, with lifetimes listed in Tables II and III. The weak dependence of τ_F on sample preparation conditions and the single-exponential form of $I_{\rm tot}(t)$ indicate that concentration-dependent processes are relatively unimportant. The ~15% decrease in the lifetime with increasing concentration could arise from a small amount of trapping by naphthalene dimers. This has been shown to have negligible influence on the fluorescence depolarization observable as long as the observed lifetime is used.[52]

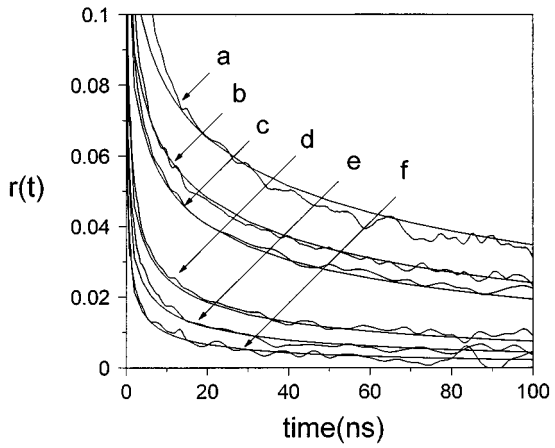

FIG. 2. Comparison of time-dependent anisotropies and EC analysis for the series *A* samples (see Table II). The initial concentration of copolymer coils is varied while the annealing time is fixed at $t_{\rm an}=20$ min. The concentrations increase with increasing rate of decay: a: 0.05%, b: 0.15%, c: 0.31%, d: 2.5%, e: 5%, f: 10%. Curve a corresponds to the intramolecular decay of the anisotropy. Subsequently faster decays of the anisotropy (curves b–f) are due to contributions from intermolecular as well as intramolecular EET. The smooth curves are the results of the EC analysis. They correspond to aggregated copolymer coils concentrated in a Gaussian volume equal to that of a single copolymer coil. The aggregation numbers are a Poisson average of ν coils per domain: a: 1, b: 3, c: 4, d: 8, e: 10, and f: 13.

Figure 2 shows anisotropy decays and calculations for the initial concentration dependent, series *A*, samples. The annealing time for these samples is $t_{\rm an}=20$ min. For all of the calculations presented here, the Poisson average number of chromophore-containing coils per domain (ν) (nanodomain concentration) was adjusted to obtain the best fit to the data. The smallest initial concentration decay ($c_0=0.05\%$) is the slowest and represents intracoil EET. The calculated line through this data corresponds to $\nu=1$. The curves that lie below represent intercoil EET for initial con-

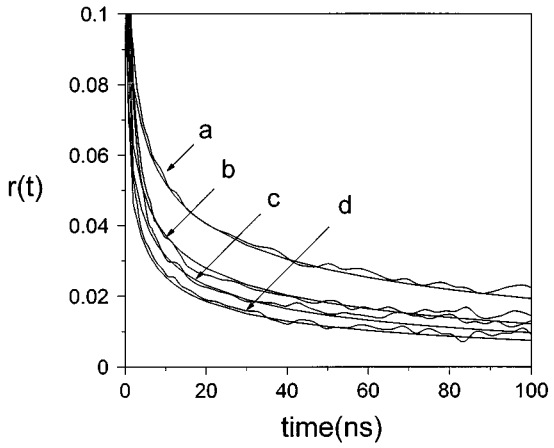

FIG. 3. Comparison of time-dependent anisotropies and EC analysis for the series *B* samples (see Table III). The initial concentration of copolymer coils is held constant (c_0=0.31%) while the annealing time is varied. The annealing times are a: 20 min, b: 1 h, c: 4 h, and d: 16 h. The smooth curves are the results of the EC analysis. They correspond to aggregated copolymer molecules concentrated in a Gaussian volume equal to that of a single copolymer coil. The aggregation numbers are a Poisson average of ν coils per domain: a: 4, b: 6, c: 7, and d: 8.

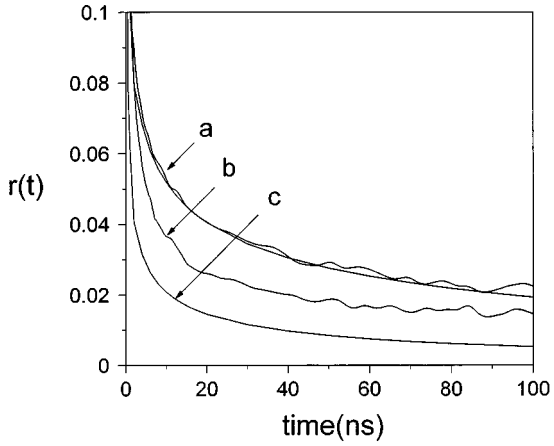

FIG. 4. Comparison of time-dependent anisotropies and EC analysis for series *B* samples. The data indicated by a and b correspond to t_{an}=20 and 60 min, respectively. The smooth curves are based on the EC analysis; however, here the concentration of the domains is held fixed while the volume is assumed to increase linearly with time. Curve a corresponds to a Poisson average of four coils in a domain with volume equal to that of a single copolymer coil. Curve c corresponds to 12 coils in a domain with volume equal to that of three times that of a single copolymer coil. These results show that a model in which the volume of the aggregate increases with time does not fit the data.

centrations c_0=0.15%, 0.31%, 2.5%, 5%, and 10%. As the initial copolymer concentration is increased, the rate of the observed EET also increases. This shows that the extent of copolymer aggregation increases monotonically with increasing c_0. The theoretical fits shown with the data correspond to ν=3, 4, 8, 10, and 13. The disagreement for the lowest concentration at short time is due to a trace fluorescent impurity in the host PVAc. The fluorescence from this impurity occurs only at very short time and is detectable for the lowest concentration samples (0.15% and 0.05%). The theoretical calculations, with one adjustable parameter, i.e., the average number of coils per aggregate, are in quantitative agreement with the data. The theory, based on a Gaussian spatial distribution of chains in the copolymer aggregate, correctly predicts both the amplitude and the functional form of the anisotropy decays.

Figure 3 shows anisotropy decays and calculations for the annealing time dependent, series *B*, samples. The initial concentration is identical for these samples, c_0=0.31%. The slowest decay corresponds to the shortest annealing time (t_{an}=20 min). Subsequently faster decays correspond to longer annealing times (t_{an}=1, 4, and 16 hr). The accompanying theoretical calculations indicate that the aggregates increase in copolymer concentration (ν=4, 6, 7, and 8) with increasing annealing time.

Although the functional agreement between the theory and data is excellent, it is necessary to compare these results with an alternative domain growth mechanism. In the above analysis, the domains are assumed to maintain a constant volume while the concentration of copolymer coils in the aggregate increases with annealing time. This situation is thought to occur during the initial stages of spinodal decomposition.[3] Another mechanism of domain growth is nucleation and growth (Ostwald ripening). Nucleation and growth describes a situation in which the local concentration of the domain remains constant while the volume grows linearly in time.[3] Figure 4 shows the annealing time-dependent data and calculations based on a nucleation and growth mechanism. The slowest decay (labeled a) corresponds to the sample annealed for 20 min and the calculation based on ν=4 chromophore-containing coils in a Gaussian domain with a volume $v_0=4\pi R_g^3/3$. The curve labeled b represents the sample annealed for 60 min. The curve labeled c is a calculation based on the nucleation and growth mechanism. This mechanism implies that the 60 min sample has ν=12 chromophore-containing coils in a Gaussian domain with a volume $3v_0$. The effect of increasing the domain volume while maintaining the local concentration overestimates the rate of the anisotropy decay. It is clear from this comparison that the nucleation and growth mechanism is inconsistent with the analysis of the annealing time-dependent data.

According to the proposed mechanism, the nanodomains occupy a volume that has approximately the same dimension as a single chromophore-containing copolymer chain. During the annealing period, those copolymer chains which approach one another within the distance $l=R_g$ form the aggregates. Each copolymer chain occupies approximately 10% of the full nanodomain volume (based on the bulk density of PMMA and PVAc, identically 1.2 g cm^{-3}). Thus, for the annealing time dependent samples, the local concentration varies between 40% and 80% chromophore-containing copolymer. It is possible to check the consistency of this model using a theory developed by Smoluchowski and later employed by Collins and Kimball to describe the kinetics of colloid coagulation as a diffusion-controlled process.[53,54] The Smoluchowski theory is based on the assumption that around a reactant particle, a concentration gradient for the other particles is set up, and the rate of flow of particles in the concentration gradient is governed by Fick's law of diffusion.

TABLE V. Values of Smoluchowski parameters for annealing time dependent, series *B*, samples. Φ is the flux of copolymer molecules across a boundary sphere of radius R, t_{an} is the annealing time, and c_0 is the initial concentration of the copolymer ($=8.85\times10^{16}$ cm^{-3}).

t_{an} (s)	$t_{an}\cdot\Phi$	$(t_{an})^{-1/2}$ ($s^{-1/2}$)	Φ (s^{-1})	$[\Phi/4\pi^{1/2}R^2c_0]$ (cm s^{-1})
1200	4	2.9×10^{-2}	3.3×10^{-3}	4.6×10^{-8}
3600	6	1.7×10^{-2}	1.7×10^{-3}	2.3×10^{-8}
14 400	7	8.3×10^{-3}	4.9×10^{-4}	6.7×10^{-9}
57 600	8	4.2×10^{-3}	1.4×10^{-4}	1.9×10^{-9}

The diffusion equation is solved with the boundary condition that the concentration is zero on the surface of a sphere of radius R, representing the distance of closest approach between two particles. The flux of particles across the boundary sphere is given by

$$\Phi = 4\pi DRc_0\left(1+\frac{R}{(\pi Dt_{an})^{1/2}}\right), \tag{4.6}$$

where D is the sum of the diffusion constants of two particles, c_0 is the initial concentration inside the sphere, and the flux is given in units of particles per second. If Eq. (4.6) is rewritten,

$$\frac{\Phi}{4\pi^{1/2}R^2c_0} = \frac{D\pi^{1/2}}{R}+\left(\frac{D}{t_{an}}\right)^{1/2}, \tag{4.7}$$

it is clear that a plot of $\Phi/4\pi^{1/2}R^2c_0$ against $(t_{an})^{-1/2}$ should be linear, if this simple model describes the copolymer aggregation.

Table V lists the values of the parameters in Eq. (4.7) corresponding to the annealing time dependent (series B) analysis. The value used for c_0 is 8.85×10^{16} cm^{-3} ($=0.31\%$) and the value used for the sphere radius, $R=R_g=34$ Å. Figure 5 shows a linear regression of the four data points. The data points fall accurately on a line ($y=mx+b$ with $m=1.81\times10^{-6}$ cm $s^{-1/2}$ and $b=-7.0\times10^{-9}$ cm s^{-1}), in agreement with the Smoluchowski model. The slope of the line is the square root of the diffusion constant. A value of $D=3\times10^{-12}$ cm^2 s^{-1} is obtained. Thus, the analysis of the series *B* samples is consistent with the interpretation that the copolymer molecules form aggregates of fixed volume and increasing concentration with time.

It is interesting to examine the predictions of the Smoluchowski equation for the series *A* samples based on the diffusion constant obtained from the above analysis of the series *B* samples. The series *B* samples were prepared with a small initial concentration, while the series *A* samples were prepared with a wide range of initial concentrations and a fixed annealing time ($t_{an}=20$ min). Equation (4.7) can be rewritten

$$\Phi = \Omega b + m\Omega(t_{an})^{-1/2}, \tag{4.8}$$

where the constants m and b are the linear regression values given above and $\Omega=4\pi^{1/2}R^2c_0$. Table VI lists values of Ω, Φ and the predicted mean number of chromophore-containing chains per domain based on the initial concentrations given in Table II. It can be seen from a comparison of the predicted and observed mean aggregation numbers that

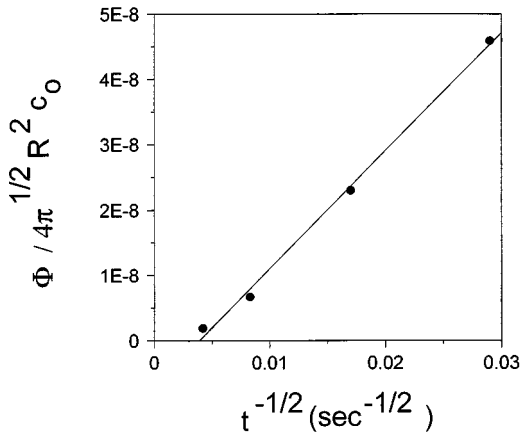

FIG. 5. The results of the EC analysis of the series *B* samples are substituted into the Smoluchowski equation [Eq. (4.7)] which describes the kinetics of colloid coagulation. The parameters corresponding to the series *B* samples are calculated in Table V. The data points are well described by the line $y=mx+b$, with $m=1.81\times10^{-6}$ cm $s^{-1/2}$ and $b=-7.0\times10^{-9}$ cm s^{-1}. The excellent agreement of the EC analysis with the Smoluchowski equation supports the nanodomain model of a constant volume (equivalent to a single copolymer coil's volume) containing an increasing number of copolymer coils. The slope of the line yields the diffusion constant of the copolymer coils, $D=3\times10^{-12}$ cm^2 s^{-1}.

the agreement is good for low initial concentrations, but is an order of magnitude off for the highest initial concentration. The diffusion constant obtained from the low c_0, series *B* samples, is too high to describe the results of the EC analysis of the higher concentration (2.5% to 10%), series *A* samples. This is not surprising, since the observed aggregation number for the 5% and 10% samples corresponds to local concentrations that are too large (100% and 130%) to be physically realistic.

There are several mechanisms that can explain the results observed for the higher concentration samples. One possibility is a change in mechanism from an increasing number of chains in a Gaussian domain of radius R_g to a mechanism akin to nucleation and growth. When the concentration of copolymer chains in a nanodomain becomes too high to permit a further increase in the number of chains within the radius R_g, the size of the nanodomain increases. It could maintain the expanded volume until it is again filled and only then increase its volume further. Alternatively, once expanded, the nanodomain could continuously increase in volume. Another possibility is that further aggregation involves the formation of larger domains from encounters between smaller ones. The nanodomains formed initially diffuse more slowly than single coils, and eventually they may aggregate to form larger clusters. This could explain the observation that the 0.31%, 16 h sample did not macroscopically phase separate, although in the cloud point study, the sample containing 2.5% copolymer became opalescent after 3 h at 65 °C. In this picture, the initial stage of phase separation is the formation of nanodomains of radius R_g. Macroscopic phase separation then requires the slow diffusion of these domains. If the sample is low concentration, the kinetics for macroscopic phase separation will be very slow, since the nanodomains will be widely separated.

TABLE VI. Values of Smoluchowski parameters for initial concentration dependent, series *A*, samples based on the diffusion constant obtained from the series *B* samples. The parameters are those defined in Eq. (4.8). Vol. % is the copolymer volume percent, c_0 is the initial concentration of the copolymer, $\Omega=4\pi^{1/2}R^2c_0$, Φ is the flux of copolymer molecules across a boundary sphere of radius R, ν (predicted) is the calculated Poisson average number of copolymer coils per domain, and ν (observed) is the mean number of coils determined from the EC analysis.

Vol. %	c_0 (cm^{-3})	Ω (cm^{-1})	Φ (s^{-1})	ν (predicted)	ν (observed)
0.05	1.48×10^{16}	12 089	5.5×10^{-4}	0.7	1
0.15	4.42×10^{16}	36 266	1.6×10^{-3}	1.9	3
0.31	8.85×10^{16}	72 533	3.3×10^{-3}	4	4
2.5	7.14×10^{17}	584 944	2.7×10^{-2}	32	8
5	1.43×10^{18}	1 169 888	5.3×10^{-2}	64	10
10	2.85×10^{18}	2 339 776	1.1×10^{-1}	132	13

V. CONCLUDING REMARKS

The theoretical analysis, based on the Gaussian coil model of the intramolecular polymer structure, quantitatively reproduces the copolymer concentration dependent and annealing time dependent energy transport measurements. These results indicate that the nanodomains occupy the same volume as a single P(MMA-2VN) coil. During the annealing period, the nanodomain volume remains fixed while the number of P(MMA-2VN) molecules increases. This observation is consistent with the predicted behavior of a spinodal decomposition mechanism. The analysis of the kinetic data agrees with the Smoluchowski model of colloid coagulation, in which the aggregation radius is equal to the radius of gyration of the copolymer. The analysis of the concentration-dependent data suggests that a different aggregation mechanism plays an important role at higher concentrations of P(MMA-2VN) ($2.5\% \leqslant c_0 \leqslant 10\%$).

It is clear that fluorescence depolarization measurements can provide a sensitive probe of aggregate formation during the initial stages of phase separation. The present study demonstrates a new method which is capable of addressing fundamental questions concerning the connection between molecular scale structure and macroscopic phase separation. We are currently studying the phase separation process from its onset through the cloud point.

ACKNOWLEDGMENT

This work was supported by the Department of Energy, Office of Basic Energy Sciences (DE-FG03-84ER13251).

[1] K. A. Peterson, M. B. Zimmt, S. Linse, R. P. Domingue, and M. D. Fayer, Macromolecules **20**, 168 (1987).
[2] M. D. Ediger, R. P. Domingue, K. A. Peterson, and M. D. Fayer, Macromolecules **18**, 1182 (1985).
[3] O. Olabisi, L. M. Robeson, and M. T. Shaw, *Polymer-Polymer Miscibility* (Academic, New York, 1979).
[4] T. Hashimoto, M. Takenaka, and T. Izumitani, J. Chem. Phys. **97**, 679 (1992).
[5] M. Takenaka, T. Izumitani, and T. Hashimoto, J. Chem. Phys. **98**, 3528 (1993).
[6] H. Jinnai, H. Hasegawa, T. Hashimoto, and C. C. Han, J. Chem. Phys. **99**, 4845 (1993).
[7] C. C. Han, M. Okada, Y. Muroga, B. J. Bauer, and Q. Tran Cong, Polym. Eng. Sci. **26**, 1208 (1986).
[8] K. Schmidt-Rohr and H. W. Spiess, in *Multidimensional Solid-State NMR and Polymers* (Academic, London, 1994).
[9] T. K. Kwei and T. T. Wang, *Polymer Blends* (Academic, New York, 1978).
[10] W. J. MacKnight and F. E. Karasz, *Comprehensive Polymer Science* (Pergamon, New York, 1989).
[11] D. Turnbull, Solid State Phys. **3**, 226 (1956).
[12] H. Tanaka, T. Hayashi, and T. Nishi, J. Appl. Phys. **65**, 4480 (1989).
[13] F. S. Bates, G. D. Wignall, and W. C. Koehler, Phys. Rev. Lett. **55**, 2425 (1985).
[14] G. D. Wignall and F. S. Bates, Makromol. Chem., Makromol. Symp. **15**, 105 (1988).
[15] A. H. Marcus, N. A. Diachun, and M. D. Fayer, Macromolecules **26**, 3041 (1993).
[16] K. U. Finger, A. H. Marcus, and M. D. Fayer, J. Chem. Phys. **100**, 271 (1994).
[17] A. H. Marcus, N. A. Diachun, and M. D. Fayer, J. Phys. Chem. **96**, 8930 (1992).
[18] A. H. Marcus and M. D. Fayer, J. Chem. Phys. **94**, 5622 (1991).
[19] J. D. Byers, W. S. Parsons, R. A. Friesner, and S. E. Webber, Macromolecules **23**, 1789 (1990).
[20] O. Pekcan and M. A. Winnik, Chem. Phys. **146**, 283 (1990).
[21] K. A. Peterson, A. D. Stein, and M. D. Fayer, Macromolecules **23**, 111 (1990).
[22] I. Yamazaki, N. Tamai, and T. Yamazaki, J. Phys. Chem. **94**, 516 (1990).
[23] J. M. Torkelson, Macromolecules **20**, 1860 (1987).
[24] L. P. Chang and H. Morawetz, Macromolecules **20**, 428 (1987).
[25] G. H. Fredrickson, Macromolecules **19**, 441 (1986).
[26] F. Mikes, H. Morawetz, and K. S. Dennis, Macromolecules **13**, 969 (1980).
[27] F. Amrani, J. M. Hung, and H. Morawetz, Macromolecules **13**, 649 (1980).
[28] T. Förster, Ann. Phys. **2**, 55 (1948).
[29] T. Förster, Radiation Res. Suppl. **2**, 326 (1960).
[30] H. Friebolin, *Basic One- and Two-Dimensional NMR Spectroscopy* (VCH, New York, 1993).
[31] J. B. Birks, *Photophysics of Aromatic Molecules* (Wiley-Interscience, London, 1970).
[32] D. L. Huber, Phys. Rev. B **20**, 2307 (1979).
[33] D. L. Huber, Phys. Rev. B **20**, 5333 (1979).
[34] A. Blumen, J. Chem. Phys. **72**, 2632 (1980).
[35] J. Baumann and M. D. Fayer, J. Chem. Phys. **85**, 4087 (1986).
[36] A. H. Marcus, M. D. Fayer, and J. G. Curro, J. Chem. Phys. **100**, 9156 (1994).
[37] C. R. Gochanour, H. C. Andersen, and M. D. Fayer, J. Chem. Phys. **70**, 4254 (1979).
[38] S. W. Haan and R. J. Zwanzig, J. Chem. Phys. **68**, 1879 (1978).
[39] P. G. Hoel, S. C. Port, and C. J. Stone, *Introduction to Probability Theory* (Houghton-Mifflin, Boston, 1971).
[40] P. G. de Gennes, *Scaling Concepts in Polymer Physics* (Cornell University, Ithaca, NY, 1979).
[41] P. J. Flory, J. Macromol. Sci.-Phys. **B12**, 1 (1976).
[42] J. G. Curro and K. S. Schweizer, Macromolecules **20**, 1928 (1987).
[43] J. G. Curro and K. S. Schweizer, J. Chem. Phys. **87**, 1842 (1987).
[44] P. J. Flory, *Principles of Polymer Chemistry* (Cornell University, Ithaca, NY, 1953).
[45] K. G. Honnell, J. G. Curro, and K. S. Schweizer, Macromolecules **23**, 3496 (1990).
[46] G. Qipeng, Polymer Commun. **31**, 217 (1990).

[47] D. V. O'Connor and D. Phillips, *Time-Correlated Single Photon Counting* (Academic, London, 1984).
[48] P. Debye, J. Chem. Phys. **31**, 680 (1959).
[49] V. E. Eskin and A. E. Nesterov, J. Poly. Sci., Part C **16**, 1619 (1967).
[50] P. Debye, B. Chu, and D. Woermann, J. Chem. Phys. **36**, 1803 (1962).
[51] T. Nishi, T. T. Wang, and T. K. Kwei, Macromolecules **8**, 227 (1975).
[52] M. D. Ediger and M. D. Fayer, Macromolecules **16**, 1839 (1983); M. D. Ediger, R. P. Domingue, and M. D. Fayer, J. Chem. Phys. **80**, 1246 (1984).
[53] F. C. Collins and G. E. Kimball, Ind. Eng. Chem. **41**, 2551 (1949).
[54] M. Smoluchowski, Ann. Physik **48**, 1103 (1917).